Chirped Microwave Signals Generation Using a Distributed Feedback Laser With Alternating Structure of Active- and Passive-Cavity

Changda Xu, Ya Jin, Jian Wang, Wenhui Sun, Liangming Xiong, Yinfang Chen, Wei Chen, and Ninghua Zhu, *Member, IEEE*

***Abstract*—We proposed a new type of distributed feedback laser with alternating active- and passive-cavities (APC DFB), which enjoys the same quantum well layer where the butt-joint re-growth process can be avoided. By utilizing the chirp characteristics of the APC DFB laser in a delayed self-heterodyne system, a chirped microwave signal with a sweep range up to 40 GHz and a sweep period of 25 μs is generated. The power fluctuation of the generated signal between 0-40 GHz within 30 minutes does not exceed 3 dB, and the scanning range fluctuates about 600 MHz. And experiment results show that the thermal efficiency of the current is always related to the working environment. In the static wavelength measurement, it is controlled by the injection current; when the chirped signal is generated, it is determined by the bias current. In particular, the waveform and the period as well as the sweep range of the generated chirped microwave signals can be accurately tuned by adjusting the modulating current, which has provided a deeper insight into the photonic generation of microwave signals.**

***Index Terms*—Distributed feedback laser, active- and passive-cavity, chirped microwave signals.**

I. Introduction

CHIRPED microwave signals find important applications in modern radar systems [1], wireless communication [2], medical imaging systems [3], and optoelectronic devices [4]. Conventionally, the pure electric methods including phase-locked loop (PLL) [5] and direct digital frequency synthesizer (DDS) [6] are generally adopted to generate microwave signals. However, the speed and bandwidth of electronic circuits limit its further development for wider band and higher frequency. Since a slight difference in the wavelength of the light corresponds to huge frequency offset in the microwave domain, the microwave photonic methods have attracted increasing research attention in recent years [7]–[11]. An early scheme of the microwave photonic methods was based on a five-stage DBR laser, which was adopted to directly modulate the phase region to obtain a microwave sweep source with a sweep range of 38.45 GHz and a sweep period of 5 μs [7]. In [8], a novel microwave sweep source was proposed based on an integrated mutually coupled (IMC) DFB laser, whose sweep range is between 40 GHz and 44.8 GHz. However, both structure of DBR laser and IMC DFB laser are complicated and expensive. In [9], a microwave signals up to 40 GHz was generated by two lasers, but this method is time-consuming for frequency matching and very sensitive to the external environment. Microwave signal could also be generated in the case where either Vertical cavity surface emitting lasers (VCSEL) or Fabry-Perot (FP) lasers is used. Nevertheless, due to the characteristics of the epitaxial growth mode of VCSEL, it is difficult to maintain a single transverse mode lasing and the output optical power is low [10]. Although the Fabry-Perot laser adopting the light injection method could make it lasing a single wavelength of light, its side mode suppression ratio is insufficient in many applications [11].

In this paper, we present an APC DFB laser to generate chirped microwave signals by a delayed self-heterodyne system. The APC DFB laser enjoys the same quantum well and grating structure, which is easy to manufacture and has a high process maturity. Through analyzing the performance of the APC DFB laser, we found that the thermal efficiency of the current is related to the test environment. The thermal efficiency of the current is determined by the bias current in the microwave signal generation, which ensuring the linearity of the chirped signal. The generated signals provide a sweep range over 40 GHz, where the signal frequency maintains a strong correlation with the injection current (I_i). Furthermore, the power stability and frequency stability of microwave signals have been verified. And we also demostrated the signal characteristics under different modulation rates (f_m) and different bias currents (i_b), which

Manuscript received July 18, 2021; accepted August 3, 2021. Date of publication August 10, 2021; date of current version August 24, 2021. This work was supported in part by Beijing Municipal Natural Science Foundation under Grants 4214082 and 4204112, in part by the National Key Research and Development Program of China under Grant 2019YFB2205302, and in part by the Open Projects Foundation under Grant SKLD1804 of State Key Laboratory of Optical Fiber and Cable Manufacture Technology. *(Corresponding author: Ninghua Zhu.)*

Changda Xu, Ya Jin, and Jian Wang are with the State Key Laboratory of Integrated Optoelectronics, Institute of Semiconductors, Chinese Academy of Sciences, Beijing 100083, China, and also with the University of Chinese Academy of Sciences, Beijing 100049, China (e-mail: xuchangda18@semi.ac.cn; jinya@semi.ac.cn; wangjian@semi.ac.cn).

Wenhui Sun, Yinfang Chen, Wei Chen, and Ninghua Zhu are with the State Key Laboratory of Integrated Optoelectronics, Institute of Semiconductors, Chinese Academy of Sciences, Beijing 100083, China (e-mail: whsun@semi.ac.cn; yfchen17@semi.ac.cn; wchen@semi.ac.cn; nhzhu@semi.ac.cn).

Liangming Xiong is with the State Key Laboratory of Optical Fiber and Cable Manufacture Technology, Yangtze Optical Fiber and Cable Joint Stock Limited Company, Wuhan 430073, China (e-mail: xiongliangming@yofc.com).

Digital Object Identifier 10.1109/JPHOT.2021.3103008

This work is licensed under a Creative Commons Attribution 4.0 License. For more information, see https://creativecommons.org/licenses/by/4.0/

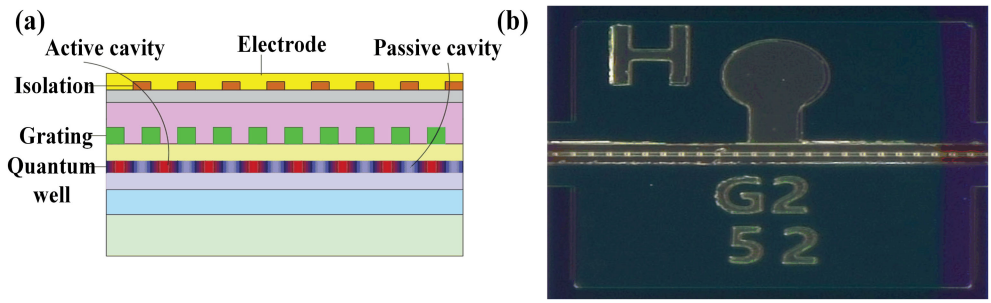

Fig. 1. The proposed APC DFB laser. (a) The structure diagram; (b) The physical image.

provides an experimental basis for dynamic adjustment of the generated microwave signals.

II. Principle

Fig. 1. (a)(b) shows the structure and physical diagram of the APC DFB laser respectively. The APC DFB laser enjoys the same quantum well layer where the butt-joint re-growth process can be avoided. A uniform grating is employed, whose structure is easy to manufacture. Generally, to impose electrical limitations on the laser in the lateral direction, the electrodes on the ridge are covered on the ohmic contact layer, and the remaining part of the electrodes are separated by the isolation layer. However, the proposed APC DFB laser is completely different. There are some electrical isolation layers on its ridges that prevent the electrodes from contacting the ohmic contact layer. Specifically, the quantum well layer corresponding to the electrical isolation layer on the ridge is called a passive cavity because it has no electrical injection and does not participate in stimulated radiation, and the active layer corresponding to the region without an electrical isolation layer participates in stimulated radiation is called an active cavity. For the APC DFB laser, the working wavelength can be tuned mainly because the current causes the change of junction temperature [12], [13], which is essentially different from the wavelength adjustment by changing the carrier concentration in [7]. Besides, the passive cavity in APC DFB lasers almost does not participate in the stimulated radiation process and forms a low-temperature region, which is conducive to heat dissipation [14]. Therefore, the wavelength largely reflects the real-time magnitude of the current, which is beneficial to keeping the change of the wavelength consistent with the change of current. Although the passive cavity will absorb photons, the output performance of proposed laser can be adjusted by controlling the position and number of passive cavities. It can be concluded from the experimental results that when the length of the periodic electrode isolation layer is less than 20 μm, and the length of the passive cavity and the active cavity is less than 3:7, the light output performance of the APC DFB laser is satisfactory.

Fig. 2. (a)(b) shows the system diagram and schematic diagram for generating frequency sweep microwave signals, respectively. By setting the parameters of the arbitrary waveform generator (AWG), a sinusoidal or triangular modulation signal with a period of T is generated. The output light of the laser is

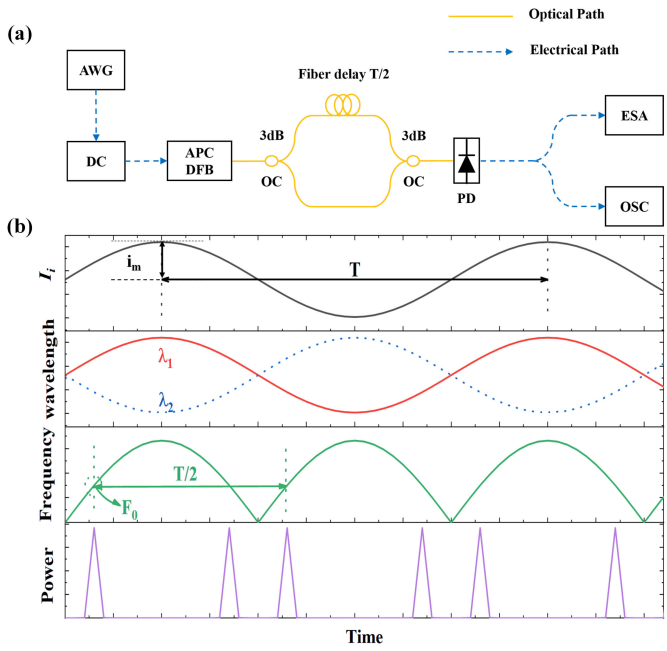

Fig. 2. Chirped microwave signals generation. (a) The experimental setup; (b) The schematic. AWG: Arbitrary waveform generator; DC: Direct current; OC: Optical coupler; PD: Photodetector; ESA: Electronic spectrum analyzer; OSC: Oscilloscope; λ_1: Light without delay; λ_2: Delayed light of T/2; F_0: Any frequency in the microwave sweep range (The purple line: the pulse cycle diagram at the F_0 frequency point).

divided into two parts, one reaches the photodetector (PD) with a delay of T/2, and the other reaches the PD without a delay. To measure the performance of the generated signal, an electronic spectrum analyzer (ESA, ROHDE&SCHWARZ) and a real-time oscilloscope (Tektronix DPO 733040D) are connected behind the PD to observe the signal. In the measurement, by adjusting the modulating currents i_{m} ($I_i = i_{\mathrm{m}} + i_{\mathrm{b}}$), the output wavelength of the laser and the beating signal are both changed. Note that the delay fiber makes the wavelength different of the two optical beams that simultaneously reach the photosensitive surface, thereby generating a higher frequency microwave signal when I_i gradually deviates from i_{b}, as shown in Fig. 2(b). In addition, the sweep period of chirped microwave signals is equal to the time interval between three adjacent pulses at the same frequency.

The output characteristics of APC DFB laser without temperature control (TEC) are shown in Fig. 3(a). The threshold

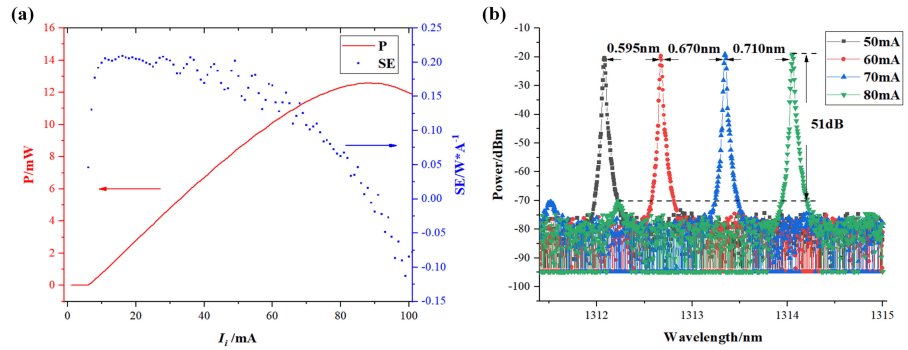

Fig. 3. The basic performance of APC DFB laser. (a) The optical power output characteristics; (b) The static wavelength drift characteristics.

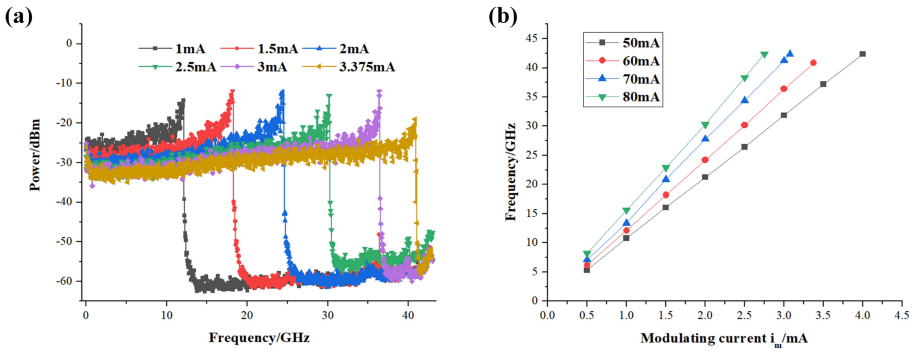

Fig. 4. Sweep frequency range under different (a) Modulating currents i_{m} from 1 to 3.375 mA and (b) Bias currents i_{b} from 50 to 80 mA.

current of the laser is about 7 mA, and the output power reaches a maximum about 13 mW at 90 mA. As the current rises, slope efficiency (SE) declines gradually during the period. Fig. 3(b) shows the wavelength static drift characteristics of our device. With the increase of the injection current, the wavelength offset caused by each 10 mA current gradually increases, which is 0.595 nm, 0.670 nm, and 0.710 nm, respectively. Since the wavelength drift of APC DFB laser is essentially the change of its junction temperature, different wavelength offsets indicate that the junction temperature changes caused by each 10 mA current are not the same. Therefore, we can conclude that the thermal efficiency of the current increases with the injection current value in the static wavelength measurement. Two main reasons could explain the slight difference about thermal efficiency. Firstly, joule heating is proportional to the square of the current; secondly, SE is also decreasing as the injection current increases. Besides, the side-mode suppression ratio of the obtained signal of the operating wavelength could reach 51 dB. It is important to pointed out that to ensure the junction temperature reached a stable level, certain injection currents value is kept unchanged more than 10 minutes during the test.

After coupling an optical signal delayed by half a period with another optical signal without delay, as shown in Fig. 2(a), the beating signal is detected by a PD with a near 40 GHz bandwidth. Fig. 4(a) shows that the sweep range increases as i_{m} increases under the condition that i_{b} is 60 mA, i_{m} is sinusoidal wave and the modulation rates ($\mathrm{f_m}$) is 20 KHz. Specifically, when i_{m} is 3.375 mA, an ultra-wide microwave frequency sweep range more than 40 GHz could be achieved. The power fluctuation of the generated signal in the whole frequency range is mainly because that the time occupied by different frequency bands is not the same. Near the highest frequency point, the corresponding wavelength change is a relatively slow and time-consuming process. So the power at highest frequencies will increase greatly. Besides, the sinusoidal modulation signal makes the generated microwave signal change slower as the frequency increases, as shown in Fig. 2(b). Consequently, this is an important reason why the power amplitude increases slowly with increasing frequency. Under the same scanning period, a smaller modulating current produces a microwave signal with a smaller scanning range, and the appearance time of the same frequency band is obviously higher than that of a microwave signal with a large scanning range. Therefore, the power of the microwave signal generated by a small modulating current is significantly higher than that generated by a large modulating current.

Fig. 4(b) shows the total influence of bias current i_{b} and modulating current i_{m} on the microwave frequency sweeping range, when the modulation period and waveform remain unchanged. Compared with the non-linear phenomenon in Fig. 3(b), the main feature of Fig. 4(b) is that the frequency change linearly with the modulating current. When the chirped signals is generated, the APC DFB laser is biased at a fixed current (i_{b}), and a relatively small current (i_{m}) modulates it. Unlike the static wavelength measurement where the current remains unchanged

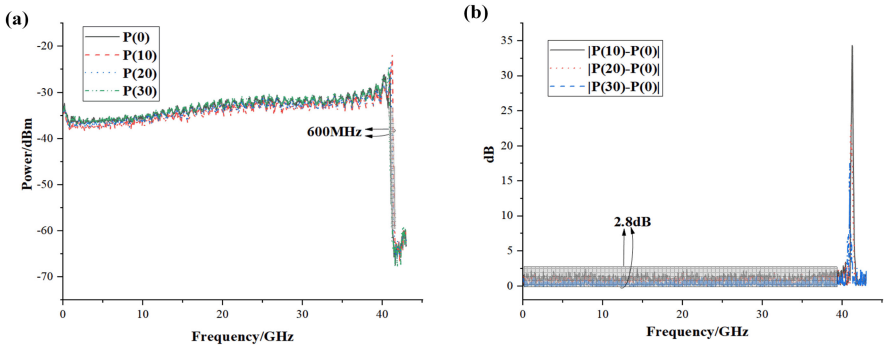

Fig. 5. The stability of the generated microwave signals. (a) The measured frequency spectrum at 010,20,30 minutes; (b) The relative change of frequency spectrum at 10,20,30 minutes.

for a long time to make the laser reach a steady state, the presence of the modulating current causes the injection current I_{i} ($I_{\mathrm{i}} = i_{\mathrm{m}}+i_{\mathrm{b}}$) to periodically change near the bias current in microwave signal generation. Since the amplitude of the modulating current is small, the thermal efficiency of the current is determined by the bias current. That is, the junction temperature has a linear relationship with the injection current, thereby ensuring the linearity of the chirped signal. It can also be seen from Fig. 4(b) that microwave signals with a sweep range over 40 GHz under different i_{b} can be obtained. Furthermore, as the i_{b} increases, the i_{m} required to reach the sweep range of 40 GHz becomes smaller. Particularly, when the bias current is 80 mA, the relationship between the frequency sweep range and the i_{m} reaches an astonishing 15 GHz/mA. Summarily, it can be seen from the dynamic (Fig. 4(b)) and static (Fig. 3(b)) wavelength drift characteristics that the thermal efficiency increases with the bias current or injection current.

The power stability and frequency stability of the chirped signal over a long period of time are measured when i_{b} is 60 mA, i_{m} is 3.375 mA and sinusoidal wave. The frequency spectrum is measured every ten minutes, and the results are P(0), P(10), P(20), P(30), respectively. It can be seen from the Fig. 5(a) that the frequency spectrum at different time has a fairly high consistency. The scanning range of the generated signal changes approximately 600 MHz within 30 minutes. In order to observe the power stability more intuitively in the time domain, the changes of the frequency spectrum at 10,20,30 minutes relative to the starting moment are obtained, as shown in Fig. 5(b). And the power fluctuation between 0-40 GHz does not exceed 3 dB.

The microwave signals under different modulating currents are captured by the oscilloscope (Tektronix DPO 733040D), and, subsequently, the time-frequency characteristics of the microwave signal are also calculated are shown in the Fig. 6. When $i_{\mathrm{m}} = 2.5$ mA, the complete time-frequency relationship of the microwave signal can be obtained. Meanwhile, when $i_{\mathrm{m}} = 3.375$ mA, the high frequency components of the generated signal are lost due to the bandwidth limitation of the real-time oscilloscope (33 GHz). In addition, at the same moment in the scanning period, the frequency of microwave signal generated by the sinusoidal wave is greater than that of the triangular wave, which is mainly caused by the difference in the modulation

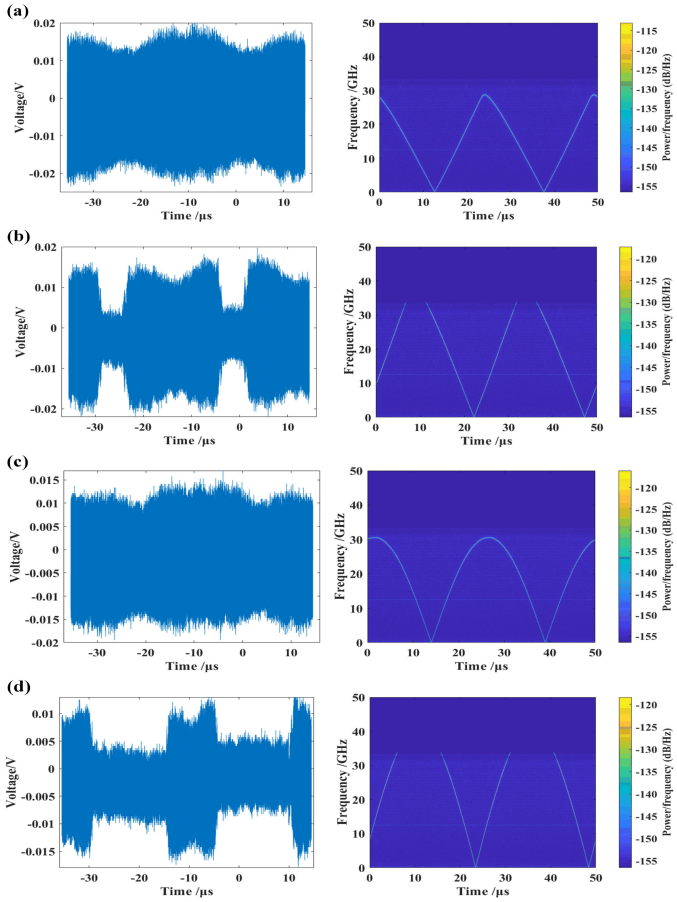

Fig. 6. Microwave signals under different modulation current waveforms and amplitudes. (a) $i_{\mathrm{m}} = 2.5$ mA, triangular wave; (b) $i_{\mathrm{m}} = 3.375$ mA, triangular wave; (c) $i_{\mathrm{m}} = 2.5$ mA, sinusoidal wave; (d) $i_{\mathrm{m}} = 3.375$ mA, sinusoidal wave.

waveform. Compared with the triangular wave, the sinusoidal wave modulating current has a larger integral over time, thus producing a wider range of junction temperature fluctuations.

The zero-frequency scan function of the ESA was used to give us knowledge of the time-frequency characteristics in the high-frequency region. Fig. 7(a) shows the pulse cycle diagram at frequency points of 10, 20 and 30 GHz when i_{m} is 3.375 mA, i_{b} is 60 mA. Closer inspection of the figure shows that the

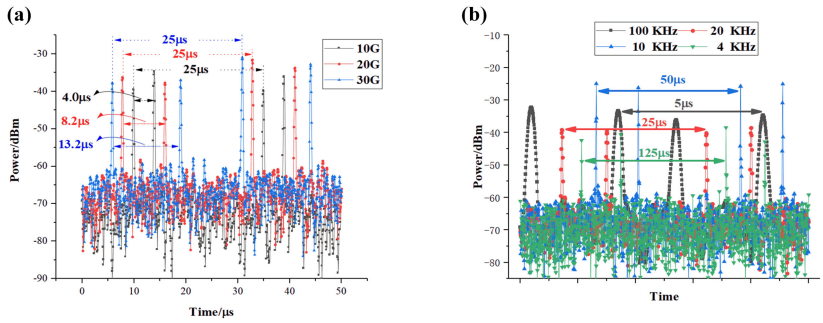

Fig. 7. The pulse period diagram at different (a) frequency points and (b) modulation rates.

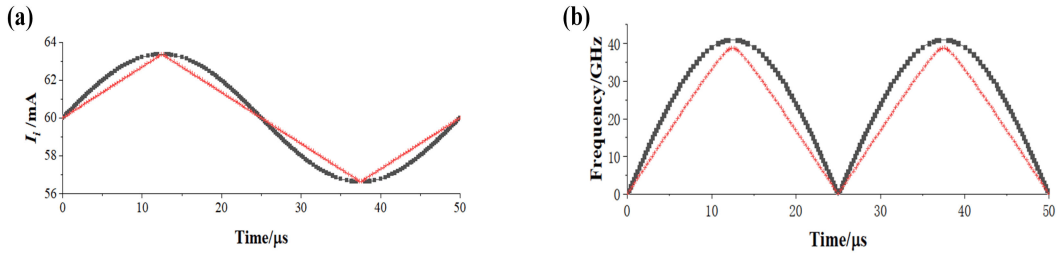

Fig. 8. The microwave signals generated under different injection current waveforms. (a) Injection current in the form of the sinusoidal wave and triangular wave; (b) Frequency-time characteristics of microwave scanning source when modulating current is sinusoidal wave and triangular wave. (Black line: the sinusoidal wave. Red line: the triangular wave).

time interval between adjacent pulses is 4, 8.2, 13.2 μs. The sweep period of different frequency points is 25 μs, which is half of the modulating current period T. Besides, the power of the microwave signal has a variation, which is mainly caused by system noise and electromagnetic field resonance. To verify the characteristics under different modulation rates, we also tested the pulse cycle diagram at frequency points of 20 GHz when the modulation rates f_m are 4 KHz, 10 KHz, 20 KHz, and 100 KHz, which is shown in Fig. 7(b). Due to the limitation of the delayed self-heterodyne system and the incident optical power of the PD (<2 dBm), different lengths of delay fibers and different fixed optical attenuators are required for different modulation rates. Therefore, the incident light power of PD changes with the modulation rate, which is the special reason for the power fluctuation in Fig. 7(b) compared to Fig. 7(a). More notably, under different modulation rates, the sweep period of the generated signal is still half of the modulating current period, which indicates that the generated microwave signals based on APC DFB lasers has good periodicity.

In the above way, pulse cycle diagrams with dozens of frequency points are carefully measured under the condition that $i_b = 60$ mA, $i_m = 3.375$ mA and $f_m = 20$ KHz. We draw the frequency change diagram of the generated microwave signal according to the time interval of the pulses at different frequencies. Fig. 8. (a)(b) shows its relationship with the injection current waveform when the injection current is sinusoidal wave and triangular wave. Specifically, except for the slowly changing around the turning point at the highest frequency, the microwave signal generated by the triangular wave changes linearly with time in the entire frequency range. Technically, we can non-linearly adjusts the triangle wave, such as slightly increasing the change rate of the injected current around the turning point, to make the generated signal have a better linear effect. It also shows that the sinusoidal wave modulation signal can generate a microwave signal with a larger scanning range, which is consistent with Fig. 6. The bandwidth and pulse duration of a chirped microwave signal generated by a sinusoidal wave can reach 40 GHz and 25 μs, respectively, which corresponds to a time bandwidth product of 1×10^6. Obviously, the waveform of the generated signal has a strong consistency with the injection current, which provides an experimental basis for generating a chirped microwave signal with a special waveform. Therefore, the proposed scheme can easily generate chirped microwave signals with tunable period, bandwidth, and waveform.

III. Conclusion

In summary, a simple and effective method for the generation of chirped microwave signals based on APC DFB laser was proposed and experimentally demonstrated. The generated microwave signals has a period of 25 μs and a bandwidth up to 40 GHz, which corresponds to a time bandwidth product of 1×10^6. The scanning range of the microwave signal changes approximately 600 MHz within 30 minutes, and the power fluctuation between 0-40 GHz does not exceed 3 dB. The experimental results also show that the current thermal efficiency is related to working conditions. The thermal efficiency of the current increases with the injection current, when measuring at static wavelength, while it is determined by the bias current in the chirped signal generation. Furthermore, the results show that the period and waveform of the generated signal have a very

strong correlation with the injection current, which indicates that various chirped microwave signals can be produced by adjusting the modulating current.

REFERENCES

[1] J. Li *et al.*, "Photonic generation of linearly chirped microwave waveforms using a monolithic integrated three-section laser," *Opt. Exp.*, vol. 26, no. 8, pp. 9676–9685, 2018.

[2] C. Wang and J. Yao, "Chirped microwave pulse compression using a photonic microwave filter with a nonlinear phase response," *IEEE Trans. Microw. Theory Techn.*, vol. 57, no. 2, pp. 496–504, Feb. 2009.

[3] H. Wang *et al.*, "Imaging biological samples using Far- and Near-Filed THz microscopy," in *Proc. 44th Int. Conf. Infrared, Millimeter, Terahertz Waves*, 2019, pp. 1–3.

[4] B. H. Zhang *et al.*, "Development of swept frequency method for measuring frequency response of photodetectors based on harmonic analysis," *IEEE Photon. Technol. Lett.*, vol. 21, no. 7, pp. 459–461, Apr. 2009.

[5] S. Schober and J. Choma, "A 1.25mW 0.8–28.2GHz charge pump PLL with 0.82ps RMS jitter in all-digital 40nm CMOS," in *Proc. IEEE Int. Symp. Circuits Syst.*, 2015, pp. 549–552.

[6] M. Padash, S. Toofan, and M. Yargholi, "A 9-bit, 1-giga samples per second sine and cosine direct digital frequency synthesizer," in *Proc. 22nd Iranian Conf. Elect. Eng.*, 2014, pp. 438–442.

[7] N. Zhu, Y. Du, X. Wu, J. Zheng, H. Wang, and J. Liu, "Fast tunable and broadband microwave sweep-frequency source based on photonic technology," *Sci. China*, vol. 56, no. 3, pp. 612–616, 2013.

[8] Y. Li, W. Zhao, H. Wang, Y. Mao, D. Lu, and Q. Kan, "Photonic generation of linearly chirped microwave waveform based on an integrated mutually coupled distributed feedback lasers," in *Proc. Asia Commun. Photon. Conf.*, 2020, pp. 1–3.

[9] J. M. Wun, C. C. Wei, J. Chen, C. S. Goh, S. Y. Set, and J. W. Shi, "Photonic chirped radio-frequency generator with ultra-fast sweeping rate and ultra-wide sweeping range," *Opt. Exp.*, vol. 21, no. 9, pp. 11475–11481, 2013.

[10] A. Malacarne *et al.*, "A ultrawide-band VCSEL-based radar-over-fiber system," in *Proc. Int. Topical Meeting Microw. Photon.*, 2019, pp. 1–4.

[11] B. Nakarmi, H. Chen, Y. H. Won, and S. Pan, "Microwave frequency generation, switching, and controlling using single-mode FP-LDs," *J. Lightw. Technol.*, vol. 36, no. 19, pp. 4273–4281, 2018.

[12] B. R. Bennett, R. A. Soref, and J. A. Del Alamo, "Carrier-induced change in refractive index of InP, GaAs and InGaAsP," *IEEE J. Quantum Electron.*, vol. 26, no. 1, pp. 113–122, Jan. 1990.

[13] G. Darvish, M. K. Moravvei-Farshi, A. Zarifkar, and K. Saghafi, "Precompensation techniques to suppress the thermally induced wavelength drift in tunable DBR lasers," *IEEE J. Quantum Electron.*, vol. 44, no. 10, pp. 958–965, Oct. 2008.

[14] X. Chen, L. Cheng, D. Guo, J. Li, and F. Choa, "Heat dissipation consideration of high-power mid-infrared quantum cascade laser arrays," in *Proc. Conf. Lasers Electro-Opt.*, 2012, pp. 1–2.